

# Journal of Biomedical Optics

BiomedicalOptics.SPIEDigitalLibrary.org

## ***In vitro* study of the erbium:yttrium aluminum garnet laser cleaning of root canal by the use of shadow photography**

Peter Gregorčič  
Nejc Lukač  
Janez Možina  
Matija Jezeršek

# *In vitro* study of the erbium:yttrium aluminum garnet laser cleaning of root canal by the use of shadow photography

Peter Gregorčič,\* Nejc Lukač, Janez Možina, and Matija Jezeršek

University of Ljubljana, Faculty of Mechanical Engineering, Aškerčeva 6, SI-1000 Ljubljana, Slovenia

**Abstract.** Erbium:yttrium aluminum garnet laser cleaning is a promising technique in endodontic treatment. In our *in vitro* study, we measured the vapor-bubble dynamics in the root canal by using shadow photography. The canal model was made of a plastic cutout placed between two transparent glass plates. An artificial smear layer was applied to the glass to study cleaning efficiency. In our results, no shock waves have been observed, since the pulp-chamber dimensions have been in the same range as the maximum diameter of the vapor bubble. This leads to the conclusion that shock waves are not the main cleaning mechanism within our model. However, the cleaning effects are also visible in the regions significantly below the bubble. Therefore, it can be concluded that fluid flow induced by the bubble's oscillations contributes significantly to the canal cleaning. We also proposed a simple theoretical model for cleaning efficiency and used it to evaluate the measured data. © 2016 Society of Photo-Optical Instrumentation Engineers (SPIE) [DOI: 10.1117/1.JBO.21.1.015008]

Keywords: erbium:yttrium aluminum garnet laser; endodontics; lasers in medicine; optodynamics.

Paper 150465RR received Jul. 9, 2015; accepted for publication Dec. 15, 2015; published online Jan. 20, 2016.

## 1 Introduction

One of the main goals in endodontic treatment is to obtain effective cleaning and decontamination of the root canal by attacking the smear layer, bacteria, and their by-products within the root canal.<sup>1-3</sup> This is especially important since removal of pulp tissues, microorganisms, and microbial toxins from the root canal system is essential for successful endodontic treatment.<sup>4</sup> Clinically, conventional endodontic techniques use mechanical instrumentation as well as ultrasonic and chemical irrigation to debride and remove infective microorganisms from the root canal system.<sup>5</sup> However, due to the complex root canal anatomy,<sup>6</sup> common irrigants are not able to penetrate into the lateral canals and the apical ramifications. Thus, conventional techniques still fall short of completely decontaminating and removing all of the infective microorganisms and debris.<sup>7</sup> Therefore, medium-infrared lasers have been introduced as an improvement of conventional cleaning.<sup>8-12</sup>

Recent studies<sup>1,2,13,14</sup> have proved that the usage of a free-running erbium:yttrium aluminum garnet (Er:YAG) laser that radiates low-energy (20 to 60 mJ) pulses with durations below 100  $\mu$ s is a very promising technique for endodontic treatment of the root canal. Such a laser-induced irrigation is able to effectively clean the debris and smear layer with minimal or no thermal damage to organic dentinal structures.<sup>3</sup> In these procedures, the dentist first gains access to the root canal and then uses minimally invasive instrumentation for the initial cleaning. After this step, the Er:YAG pulses are delivered into the coronal portion of the pulp chamber and filled with water or sodium hypochlorite, by using fiber tips with different geometries, to perform the laser cleaning.<sup>1</sup>

Free-running Er:YAG lasers, emitting pulsed light at a wavelength of 2.94  $\mu$ m, are used for cleaning, since they have the highest absorption in water.<sup>15</sup> Due to the very high absorption coefficient,  $\mu_a = 1.247 \times 10^6 \text{ m}^{-1}$ , almost all the pulse light is absorbed within only a 1- $\mu$ m-thick water layer. Thus, the water is locally and instantly heated over the boiling point. Due to this explosive boiling, a vapor bubble is formed, and it starts to expand at the fiber tip's end.<sup>8,16,17</sup> This is a typical process, where the laser pulse energy is converted into mechanical energy of the liquid medium. When the laser pulse ends and the bubble reaches its maximum volume, it collapses due to the pressure of the surrounding liquid.<sup>18</sup> This collapse, in turn, initiates a new bubble's growth and collapse. The described bubble dynamics repeat themselves in so-called vapor bubble oscillations until the bubble's mechanical energy is dissipated.<sup>17,19</sup>

In our previous study,<sup>17</sup> we examined how fiber tip geometry influences the vapor bubble's dynamics in an infinite liquid. However, during endodontic treatment, the bubble is formed within a confined geometry, limited by the root canal's boundaries. In this case, the bubble's expansions and collapses induce fluid streaming that could explain the cleaning efficiency of the laser-induced irrigation. However, the principles of the cleaning mechanisms are still not well explained.<sup>9</sup> Therefore, the main aim of this paper is to use shadow photography to study cleaning efficiency in a model of a root canal, made of a plastic cutout placed between two transparent glass plates and coated by an artificial smear layer.

## 2 Materials and Methods

### 2.1 Root Canal Model

The vapor bubble's dynamics and cleaning efficiency were investigated in the model of the root canal shown in Fig. 1.

\*Address all correspondence to: Peter Gregorčič, E-mail: [peter.gregorcic@fs.uni-lj.si](mailto:peter.gregorcic@fs.uni-lj.si)

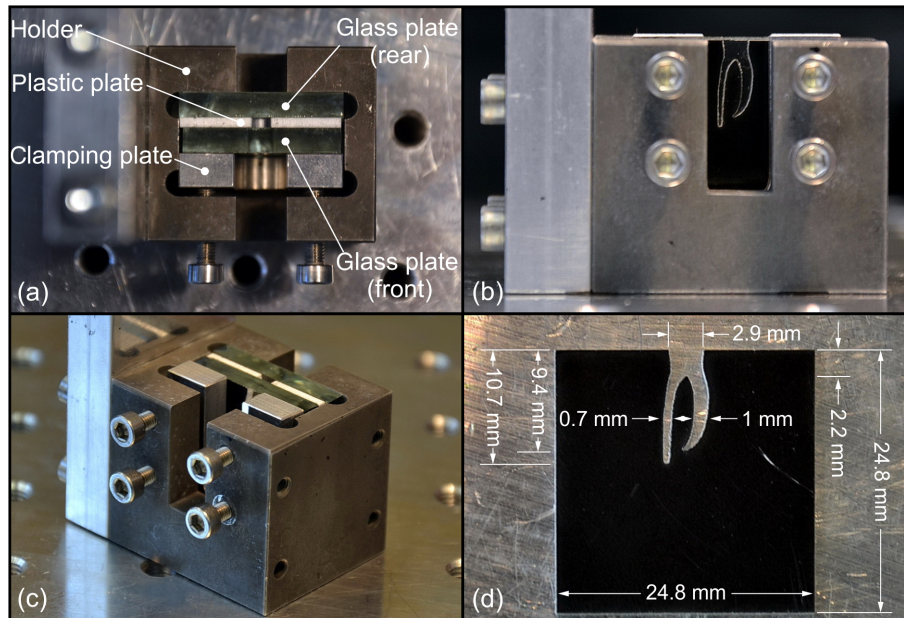


**Fig. 1** An *in vitro* model of the root canal: (a) the top view explaining the canal model components, (b) the front view, (c) the isometric view, and (d) a plastic cutout of the root canal with dimensions; the thickness of a plastic plate equals 1.5 mm.

Since we used a shadowgraphic observation technique,<sup>17</sup> the front and the rear surfaces of the canal model were made of flat and transparent material. Thus, we built a model of a plastic plate [e.g., see Fig. 1(d)] placed between two transparent glass plates, as shown in Figs. 1(a) and 1(c). They were clamped together by an aluminum clamping plate placed into an aluminum holder, as visible in Figs. 1(a)–1(c). The thickness of the plastic plate was 1.5 mm. The pulp chamber and two canals were cut from this plate with the dimensions that are shown in Fig. 1(d). The model was submerged into water and illuminated by an illumination pulse used for shadowgraphy, as described in Sec. 2.2.

## 2.2 Experimental Setup for Shadowgraphic Observations

The experimental setup is shown in Fig. 2. The holder with the model of the root canal, described in Sec. 2.1, was submerged into a vessel with distilled water 10 mm under the water level to ensure that the canal is filled with water during the entire series of the experiments. A free-running Er:YAG laser, designed

for laser dentistry ( $\lambda = 2.940 \mu\text{m}$ , Fotona d.d., Slovenia, LightWalker), was used as the excitation source. We used pulses with durations of  $100 \mu\text{s}$  and pulse energies (at the output of the fiber tip) of 54 mJ. The pulse repetition rate was 15 Hz. Typical excitation pulse power as a function of time for the laser used in our experiments can be found elsewhere.<sup>17</sup>

The delivery of the laser pulse into the pulp chamber of the canal model was performed by using a fiber tip. The fiber tip was placed into the center of the pulp chamber, 1.6 mm below the top of the model, as visible from Fig. 3(a1). For our experiments, we used a Fotona Xpulse 400/14 fiber tip, schematically shown on the right-hand side of Fig. 2. The fiber tip was 14 mm long with a diameter of  $470 \mu\text{m}$  and tapered at an angle of 27 deg.

The vapor bubble's dynamics and the cleaning efficiency were studied by using shadowgraphy. We used the same system for shadowgraphy as described in detail in Ref. 17. As the illuminating source we used a frequency-doubled Nd:YAG laser (Ekspla, Lithuania, PL2250-SH-TH) emitting green ( $\lambda = 532 \text{ nm}$ ) pulses with durations of 30 ps. A beam expander was used to expand the illuminating beam so that the whole area

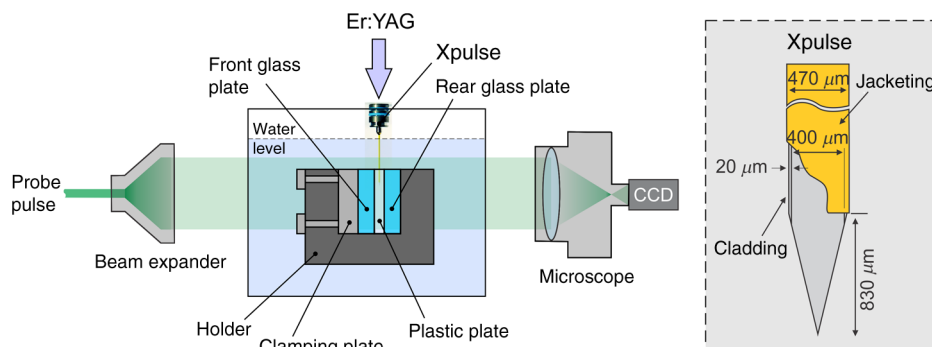


**Fig. 2** Schematic view of the experimental setup.

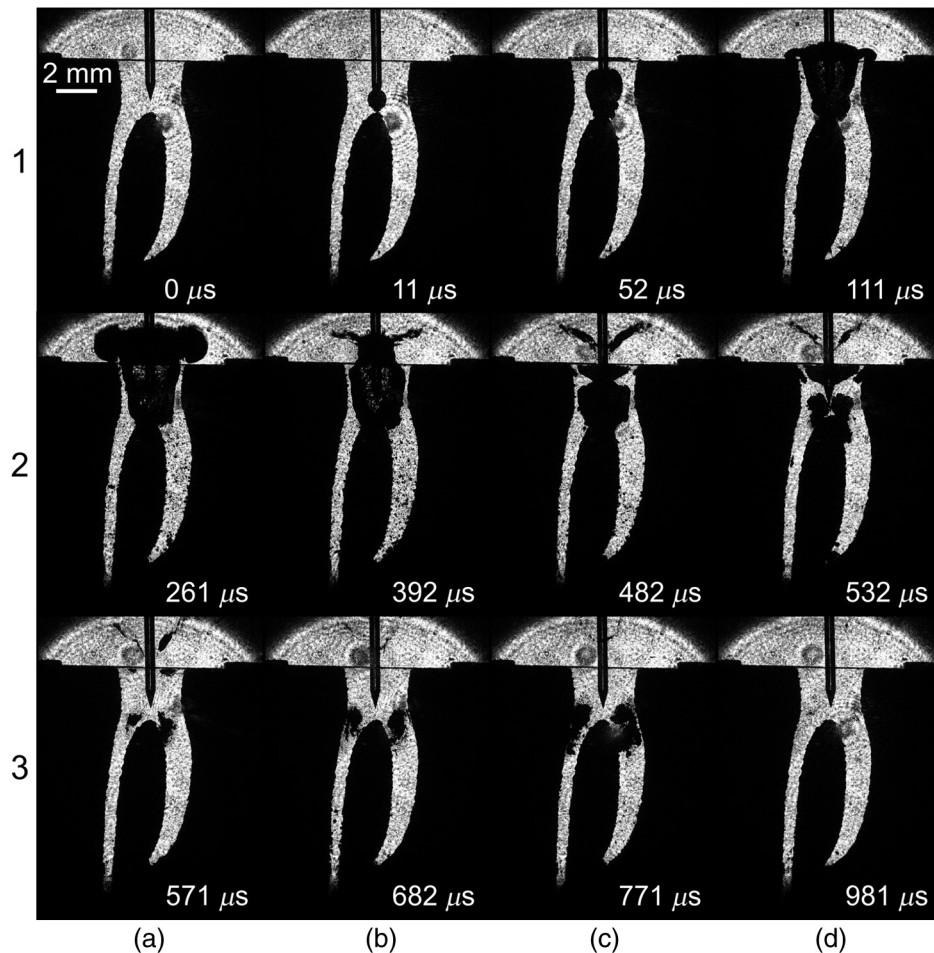


**Fig. 3** A series of typical images (Video 1) of a vapor bubble induced by the Er:YAG laser in the model of the root canal. The scale is shown in the upper-left corner of (a1). The time after the pulse initiation is shown on the bottom-right side of each image. (Video 1, MPEG, 10.1 MB) [URL: <http://dx.doi.org/10.1117/1.JBO.21.1.015008.1>].

of the root canal model was illuminated. Images were captured through a microscope equipped with a charge-coupled device (CCD) camera (Basler AG, Germany, scA1400-17fm, 1.4 Mpx). Since the illuminating beam diameter was smaller than the field of view of the optical system, a bright circular area appears in the captured shadowgraphs [e.g., see Fig. 3(a1)].

### 2.3 Measurements of the Bubble's Dynamics

For the measurements of the vapor bubble's dynamics in the root canal, we used clean and transparent glass plates. The excitation laser, illumination laser, and CCD camera were synchronized with a signal generator (Tektronix, US, AFG 3102) connected to a PC. The experimental setup was automatically controlled with custom-developed software, written in MATLAB<sup>®</sup>, which also enables the setting of the excitation laser's parameters, image acquisition, and image processing.

The bubble's dynamics were measured by capturing a series of shadowgraphic images. Each image was captured at a different delay between the excitation and the illumination pulse. For each image, a new event was needed, and thus, repeatable conditions had to be ensured.

### 2.4 Measurements of Cleaning Efficiency

In the experiments devoted to the study of cleaning efficiency, we applied the artificial smear layer in the front glass surface of the canal. As an artificial smear layer we used a black paint that does not dissolve in water and can be mechanically removed. In these experiments, we measured the transmittance of the illumination pulse versus the total pulse energy applied into the canal as follows.

In each step, we applied seven pulses with frequency of 15 Hz into the canal. This was repeated until the canal was completely cleaned. After each step of seven pulses, we waited for 5 s so that the vapor bubble and the remaining gas bubbles were not present and visible any more. Then we illuminated the canal by an illumination pulse and captured an image.

To confirm repeatability, the entire procedure of cleaning the canal, described in the above paragraph, was repeated 10 times. Before each iteration, the canal model was completely mechanically cleaned and then painted with a fresh coat of paint before performing a new series of experiments.

The acquired images were processed by the custom-developed software to calculate transmittance. The total pixel intensity  $I$  of each image was calculated as

$$I = \sum_{i=1}^w \sum_{j=1}^h P_{ij}, \quad (1)$$

where  $w = 1040$  px and  $h = 1392$  px stand for the image width and height, respectively. The single-pixel intensity  $P_{ij}$  is an integer between 0 and 255, since we used 8-bit pixel depth. Thus, a value of 0 means a black pixel, while a value of 255 corresponds to a white pixel.

The transmittance  $T_N$  after the  $N$ th pulse, therefore, equals

$$T_N = \frac{I_N - I_0}{I_\infty}. \quad (2)$$

Here,  $I_N$  stands for the total pixel intensity [defined by Eq. (1)] of the image acquired after the  $N$ th pulse,  $I_0$  is the total pixel intensity for the image captured before the first Er:YAG pulse, and  $I_\infty$  stands for the total pixel intensity of the image captured when the canal is completely cleaned.

The total pulse energy  $E$  was measured as

$$E = N_p E_p. \quad (3)$$

Here,  $E_p = 54$  mJ stands for the energy of a single pulse, and  $N_p$  is the number of pulses already applied into the canal.

### 3 Results and Discussion

#### 3.1 Bubble's Dynamics in the Root Canal

In the first series of our experiments, we captured the bubble's dynamics in the canal. Thus, both the front and the rear glass plates were kept clean during these experiments. A typical series of images of the bubble, captured at different times after the beginning of the Er:YAG laser pulse, is shown in Fig. 3.

The Er:YAG pulse, having a wavelength of  $\lambda = 2.940 \mu\text{m}$ , is completely absorbed right beside the fiber tip due to the very high absorption coefficient,  $\mu_a = 1.247 \times 10^6 \text{ m}^{-1}$ .<sup>15</sup> This results in the laser energy deposition causing an explosive boiling, and the spherical bubble develops at the end of the conical fiber tip<sup>17</sup> [e.g., see Fig. 3(b1)]. The spherical geometry of the bubble is deformed during the bubble's expansion due to the influence of the confined geometry of the canal, as visible from Figs. 3(a2), 3(c1), and 3(d1). For the parameters used in our experiments, the bubble reaches its maximum volume around 260  $\mu\text{s}$  after the pulse initiation [Fig. 3(a2)]. Then it starts to collapse due to the pressure of the surrounding liquid. During the collapse, it decays into two bubbles, as visible from Figs. 3(d2) and 3(a3). These bubbles oscillate several times in the top part of the canal until they disappear due to mechanical-energy dissipation. This happens around 1 ms after the pulse initiation [e.g., see Fig. 3(d3)].

As we have already shown in Ref. 17, the acoustic transient, or shock wave, is not emitted during the first bubble's expansion, since the Er:YAG laser energy is deposited into water within a time that is three orders of magnitude longer<sup>17,20</sup> than the characteristic time for the propagation of stress waves across the irradiated volume.<sup>21–23</sup> Although in an infinite liquid shock waves are emitted during the vapor bubble's collapses,<sup>17</sup> this is not the case for the bubble oscillating within our canal model. In this case, the canal's boundaries decelerate the bubble's collapse,<sup>24</sup> and therefore, the shock waves are not emitted even during the bubble's collapses. This finding is important, since it leads to the conclusion that shock waves do not

explain the cleaning mechanism of the Er:YAG laser irrigation, as suggested in Refs. 1, 2, and 11.

It should be noted here that in the case when the dimensions of the pulp chamber would be several times larger than the maximum diameter of the vapor bubble, shock waves could be induced during the bubble's collapses as is the case for the infinite liquid. However, we have chosen smaller dimensions of the pulp chamber to eliminate the influence of the secondary shock waves. Since the shock waves are not induced in our case, while the canal is still cleaned, we believe that they do not represent the main cleaning mechanism.

A series of typical images of a vapor bubble in the root canal reveals that the laser-induced vapor bubble oscillates only in the pulp chamber and in the top part of both canals. Thus, this bubble does not reach the bottom part of the canal (e.g., see Fig. 3). This leads to the conclusion that the laser-induced vapor bubble itself cannot be the direct canal-cleaning mechanism. However, many small gas bubbles appear within the whole canal during the vapor bubble expansion and collapse and are clearly visible in Video 1. We believe that they appear due to the shear stress on the canal walls caused by dynamic viscosity of the fluid streaming that is induced by the main vapor bubble's oscillations. These small, submillimeter, or even submicrometer gas bubbles may also significantly contribute to the cleaning of the smear layer from the canal walls,<sup>25–27</sup> especially when they appear in the close vicinity of the smeared surface.<sup>28</sup>

#### 3.2 Ability of Shadowgraphy to Detect the Shock Waves

In Sec 3.1, we have shown that the shock waves are not presented during the bubble's oscillations within the root canal. To confirm that this finding is not affected by the potential inability of the shadowgraphy to detect the shock waves, we made additional verification experiments in an infinite liquid. We chose the nonconfined geometry, since it has been already shown<sup>17</sup> that in an infinite liquid, the shock waves are induced by the bubble's rebound. For verification reasons, we used the same fiber tip and the same laser pulse parameters as in the case of bubble dynamics measurements within the canal. The verification experiments confirmed that the shock waves can be easily observed by our method, as is clearly seen from Fig. 4.

The results of our verification experiment in an infinite liquid show that our experimental system is able to observe the shock waves. This confirms our result—presented in Sec 3.1—that shock waves do not appear within our root canal due to the confined geometry.

#### 3.3 Cleaning Efficiency

For the study of cleaning efficiency, we applied an artificial smear layer (i.e., the black paint described in Sec. 2.4) to the front glass surface of the canal, and we measured how this smear layer was removed during the Er:YAG pulses application. A typical series of images showing the smear layer removal by laser-induced streaming is presented in Fig. 5. Each subsequent image was captured after the additional seven Er:YAG pulses were delivered into the canal. The total pulse energy already delivered into the canal was calculated using Eq. (3) and is shown on the bottom-right side of each image in Fig. 5.

From Fig. 5, we can see that in this particular case, the canal was almost cleaned (>85%) when the total pulse energy of  $\sim 5.4$  J was applied into the water. It should be noted here

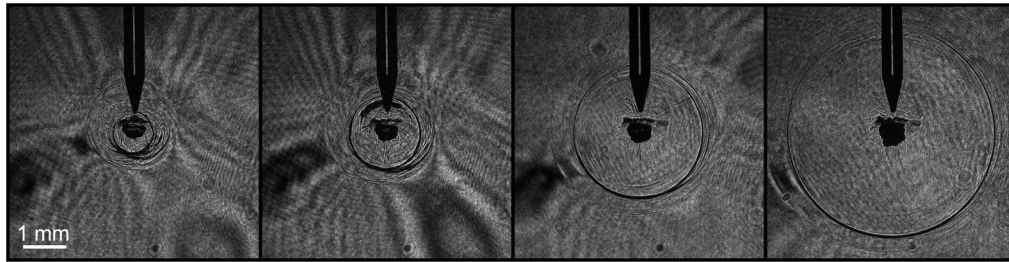


**Fig. 4** A series of shock waves, observed during the first bubble rebound ( $\sim 500 \mu\text{s}$  after the pulse initiation) in the verification experiment, where the Er:YAG pulse was delivered into a nonconfined liquid.

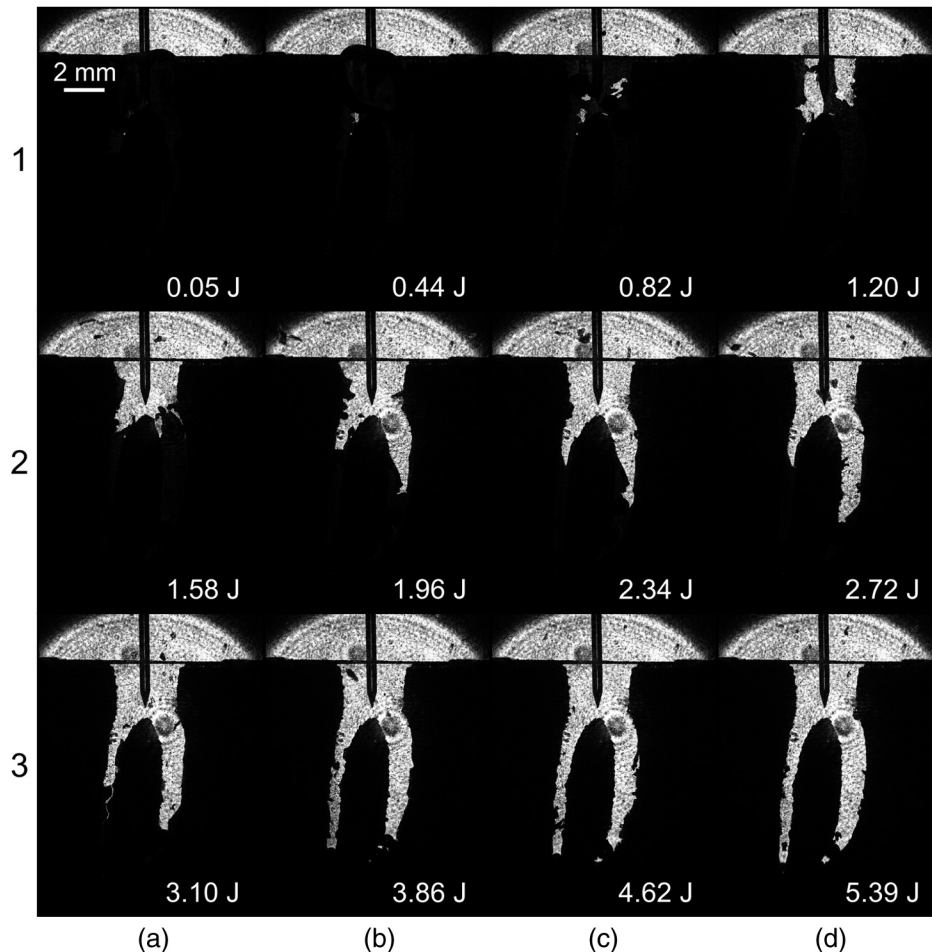


**Fig. 5** A series of typical images (Video 2) showing the cleaning efficiency as a function of the total pulse energy applied into the canal. Here, the total pulse energy is calculated from the number of pulses by using Eq. (3). The scale is shown in the upper-left corner of (a1). (Video 2, MPEG, 3.62 MB) [URL: <http://dx.doi.org/10.1117/1.JBO.21.1.015008.2>].

that small black areas in the bottom of both canals in Fig. 5(d3) do not correspond to the smear layer. Instead, they appear due to small gas bubbles that are formed because of the main vapor bubble's oscillations as explained in Sec. 3.1. They can be clearly recognized from Video 2.

From the results presented in Fig. 5, it can be concluded that the cleaning effects appear along the entire canal, that is, also significantly below the regions that are reached by the laser-induced vapor bubble (e.g., compare Figs. 3 and 5). Therefore, we believe that (1) water flow, induced by the dynamics of a laser-induced vapor bubble, and (2) gas bubbles appearing

along the whole canal are responsible for the cleaning. The water-flow cleaning and the gas bubbles' appearance probably happen through the shear stress caused by the dynamic viscosity.

From the images acquired during the study of cleaning efficiency (e.g., presented in Fig. 5), we calculated the transmittance by using Eq. (2). The average transmittance as a function of the total pulse energy, defined by Eq. (3), is shown in Fig. 6. Each point corresponds to the average of 10 independent measurements, and the vertical bars show standard deviations. From the results in Fig. 6, it can be seen that, on average, up to

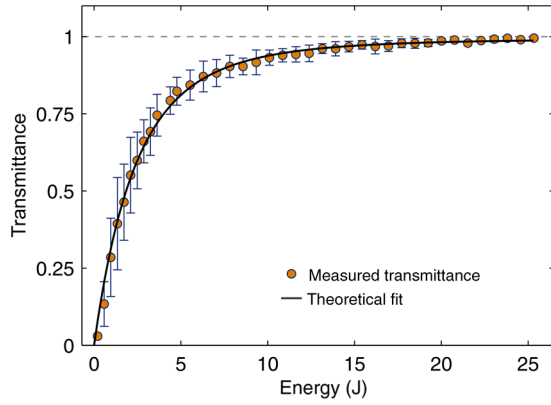


**Fig. 6** The transmittance [defined by Eq. (2)] as a function of the total energy [defined by Eq. (3)]. When the transmittance reaches unity, the canal is totally cleaned. The dots show an average value of 10 independent measurements, while the standard deviations are presented by vertical lines. The fit of the theoretical model [Eq. (8)] is shown by the black curve.

25 J (i.e., ~460 pulses) are needed to completely clean our *in vitro* model of the root canal.

The cleaning efficiency can be modeled as follows. The small area of the smear layer  $dA$  that is removed by the delivery of a small amount of the laser pulse energy  $dE$  is proportional to the area  $A$  that is still smeared:

$$dA = -A\alpha(E)dE. \quad (4)$$

In our approximation, we assumed that the positive rate  $\alpha$ , that is, the cleaning efficiency coefficient, decreases with the total energy  $E$  that has already been applied into the canal and has already contributed to the canal cleaning as

$$\alpha(E) = \alpha_0 e^{-\beta E}. \quad (5)$$

Here,  $\alpha_0$  stands for the cleaning efficiency coefficient at the beginning of the cleaning process and  $\beta$  is a positive constant.

Combining Eqs. (4) and (5), after integration, one can obtain the dependence of the still-smear area  $A_S$  as a function of the total pulse energy  $E$ :

$$A_S = A_0 \exp \left[ -\frac{\alpha_0}{\beta} (1 - e^{-\beta E}) \right]. \quad (6)$$

Here,  $A_0$  stands for the smear layer area before the first pulse application (i.e., at  $E = 0$ ).

If one assumes that the cleaning efficiency coefficient stays constant during the entire cleaning procedure, that is, in the case of the limit conditions of  $\beta \rightarrow 0$ , Eq. (6) is simplified to  $A_S(E) = A_0 e^{-\alpha_0 E}$ . In this case, a more intuitive characteristic coefficient of the cleaning efficiency, the half-energy  $E_{1/2}$ , can be defined as the total energy required for the cleaning of one half of the initial smear layer area:

$$E_{1/2} = \frac{\ln(2)}{\alpha_0}. \quad (7)$$

The transmittance  $T$ , defined by Eq. (2), is equal to the ratio between the cleaned area  $A_C = A_0 - A_S$  and the area  $A_0$  of the smear layer before the first pulse application:  $T = (A_0 - A_S)/A_0 = 1 - (A_S/A_0)$ . Thus, by using Eq. (6), the transmittance as a function of the total pulse energy  $E$  can be modeled as

$$T = 1 - \exp \left[ -\frac{\alpha_0}{\beta} (1 - e^{-\beta E}) \right]. \quad (8)$$

The fit of Eq. (8) to the measured data is shown by the black curve in Fig. 6. In such a way, we measured the cleaning efficiency coefficient to be  $\alpha_0 = 0.4 \text{ J}^{-1}$ , while its dependence on the total pulse energy is weak, resulting in a low coefficient  $\beta = 0.08 \text{ J}^{-1}$ . Therefore, the half-energy, defined by Eq. (7), in our case can be estimated to  $E_{1/2} = 1.7 \text{ J}$  (and it equals to ~30 pulses).

## 4 Conclusions

By using shadow photography, we performed an *in vitro* study of the Er:YAG laser cleaning of the root canal. Here, we studied the vapor bubble's dynamics and cleaning efficiency in the model of the root canal.

The results of the bubble's dynamics, measured in a canal that was made of a plastic cutout placed between two transparent glass plates, show that the vapor bubble appears only in the top part of the canal. Our results reveal that for the vapor bubble oscillating within the canal, shock waves are not present either at the first bubble's expansion or during its collapses (contrary to the case for the bubble oscillating in an infinite liquid). This finding leads to the conclusion that shock waves do not contribute significantly to the Er:YAG laser cleaning mechanisms.

The artificial smear layer was applied to the front glass surface of the canal model for studying the cleaning efficiency. The obtained results show that the cleaning effects appear along the entire canal, that is, also in the bottom part of the canal, which is not reached by the laser-induced vapor bubble. This leads to the conclusion that the vapor bubble itself is not the direct cleaning mechanism. Instead, the fluid streaming that is induced by the bubble's oscillations contributes to the canal cleaning. Consequently, small gas bubbles that can also contribute to the canal cleaning are induced along the whole canal. We believe that this happens through the shear stress on the canal's walls caused by dynamic viscosity. However, several questions still remain open. One of the most important open issues is the explanation of the mechanisms of cleaning of the small lateral channels with radii of several tens of micrometers.

We also measured the cleaning effects as a function of the total pulse energy applied into the canal. Here, we proposed a simple model assuming that the amount of smear layer removed by the pulse energy is proportional to the current smear layer area. The results show that the half-energy, that is, the total energy that is required for the cleaning of one half of the initial smear layer area, in our case, equals 1.7 J.

## Acknowledgments

We would like to thank Fotona, d.d. for supplying their commercially available laser system for laser cleaning of the root canals in clinical dentistry applications. Their system including the Er:YAG laser (LightWalker), handpiece, and interchangeable fiber tips was used as an excitation source in our experiments.

## References

1. G. Olivi and E. DiVito, "Photoacoustic endodontics using PIPST<sup>TM</sup>: experimental background and clinical protocol," *J. Laser Health Acad.* **2012**(1), 22–25 (2012).
2. E. DiVito, O. A. Peters, and G. Olivi, "Effectiveness of the erbium:YAG laser and new design radial and stripped tips in removing the smear layer

- after root canal instrumentation," *Lasers Med. Sci.* **27**(2), 273–280 (2012).
3. S. Sahar-Helft et al., "Effect of Er:YAG laser-activated irrigation solution on *Enterococcus faecalis* biofilm in an ex-vivo root canal model," *Photomed. Laser Surg.* **31**(7), 334–341 (2013).
  4. C. L. Basmadjian-Charles et al., "Factors influencing the long-term results of endodontic treatment: a review of the literature," *Int. Dent. J.* **52**(2), 81–86 (2002).
  5. L. S. Gu et al., "Review of contemporary irrigant agitation techniques and devices," *J. Endodont.* **35**(6), 791–804 (2009).
  6. O. A. Peters, "Current challenges and concepts in the preparation of root canal systems: a review," *J. Endodont.* **30**(8), 559–567 (2004).
  7. T. Matsuo et al., "An immunohistological study of the localization of bacteria invading root pulpal walls of teeth with periapical lesions," *J. Endod.* **29**(3), 194–200 (2003).
  8. F. H. Takeda et al., "Efficacy of Er:YAG laser irradiation in removing debris and smear layer on root canal walls," *J. Endod.* **24**(8), 548–551 (1998).
  9. S. D. de Groot et al., "Laser-activated irrigation within root canals: cleaning efficacy and flow visualization," *Int. Endod. J.* **42**(12), 1077–1083 (2009).
  10. H. Matsumoto, Y. Yoshimine, and A. Akamine, "Visualization of irrigant flow and cavitation induced by Er:YAG laser within a root canal model," *J. Endod.* **37**(6), 839–843 (2011).
  11. D. L. Glover et al., "Laser based enhanced generation of photoacoustic pressure waves in dental and medical treatments and procedures," U. S. Patent No. US7959441 B2 (2011).
  12. M. E. Licata et al., "Effectiveness of a new method of disinfecting the root canal, using Er, Cr:YSGG laser to kill *Enterococcus faecalis* in an infected tooth model," *Lasers Med. Sci.* **30**(2), 707–712 (2015).
  13. O. A. Peters et al., "Disinfection of root canals with photon-initiated photoacoustic streaming," *J. Endod.* **37**(7), 1008–1012 (2011).
  14. E. Deleu, M. Meire, and R. G. Moor, "Efficacy of laser-based irrigant activation methods in removing debris from simulated root canal irregularities," *Lasers Med. Sci.* **30**(2), 831–835 (2015).
  15. G. M. Hale and M. R. Querry, "Optical-constants of water in 200-nm to 200- $\mu$ m wavelength region," *Appl. Opt.* **12**(3), 555–563 (1973).
  16. A. Vogel and V. Venugopalan, "Mechanisms of pulsed laser ablation of biological tissues," *Chem. Rev.* **103**(2), 577–644 (2003).
  17. P. Gregorčič, M. Jezeršek, and J. Možina, "Optodynamic energy-conversion efficiency during an Er:YAG-laser-pulse delivery into a liquid through different fiber-tip geometries," *J. Biomed. Opt.* **17**(7), 075006 (2012).
  18. P. Gregorčič et al., "Measurements of cavitation bubble dynamics based on a beam-deflection probe," *Appl. Phys. A* **93**(4), 901–905 (2008).
  19. P. Gregorčič et al., "Synchronized delivery of Er:YAG-laser-pulse energy during oscillations of vapor bubbles," *J. Laser Health Acad.* **2014**(1), 14–19 (2014).
  20. M. Frenz et al., "Starting mechanisms and dynamics of bubble formation induced by a Ho:yttrium aluminum garnet laser in water," *J. Appl. Phys.* **84**(11), 5905–5912 (1998).
  21. S. L. Jacques, "Role of tissue optics and pulse duration on tissue effects during high-power laser irradiation," *Appl. Opt.* **32**(13), 2447–2454 (1993).
  22. R. O. Esenaliev et al., "Studies of acoustical and shock-waves in the pulsed-laser ablation of biotissue," *Lasers Surg. Med.* **13**(4), 470–484 (1993).
  23. E. D. Jansen et al., "Effect of pulse duration on bubble formation and laser-induced pressure waves during holmium laser ablation," *Laser Surg. Med.* **18**(3), 278–293 (1996).
  24. E. A. Brujan et al., "The final stage of the collapse of a cavitation bubble close to a rigid boundary," *Phys. Fluids* **14**(1), 85–92 (2002).
  25. C. D. Ohl et al., "Surface cleaning from laser-induced cavitation bubbles," *Appl. Phys. Lett.* **89**(7), 074102 (2006).
  26. A. Agarwal et al., "Biofilm detachment by self-collapsing air microbubbles: a potential chemical-free cleaning technology for membrane biofouling," *J. Mater. Chem.* **22**(5), 2203–2207 (2012).
  27. G. M. Liu and V. S. J. Craig, "Improved cleaning of hydrophilic protein-coated surfaces using the combination of nanobubbles and SDS," *ACS Appl. Mater. Interfaces* **1**(2), 481–487 (2009).
  28. M. Hauptmann et al., "Importance of bubble size control in ultrasonic surface cleaning by pulsed high-frequency sound fields," *ECS J. Solid State Sci. Technol.* **3**(1), N3032–N3040 (2014).

**Peter Gregorčič** received his PhD in physics from University of Ljubljana, Slovenia, in 2012. Currently, he is working as an assistant professor for laser applications at the Faculty of Mechanical Engineering, University of Ljubljana. Within the research fields of optodynamics and laser applications, he is mainly focused on research and development of the laser medicine, laser processing systems and interactions, methods of online measurements, and laser-induced surface microstructures.

**Nejc Lukač** is a PhD student at the Faculty of Mechanical Engineering, University of Ljubljana. His main topics of research are the use of lasers and laser pulse shaping in medical applications. He is currently employed at Fotona d.o.o.

**Janez Možina** is a full professor for physics and laser applications at the Faculty of Mechanical Engineering, University of Ljubljana. He is the founder and head of chair of optodynamics and laser applications. He introduced a new research field, optodynamics, dealing with the dynamic aspects of light-matter interaction. He has been a coauthor of more than 150 scientific papers published in scientific journals.

**Matija Jezeršek** is an associate professor for laser applications at the Faculty of Mechanical Engineering, University of Ljubljana. He received his PhD in mechanical engineering in 2004. His major research interests include 3-D optical metrology, laser processing, and research of optodynamic phenomena.